Improved near real time surface wind resolution over the Mediterranean Sea

A. Bentamy, H.-L. Ayina, P. Queffeulou, D. Croize-Fillon

Ocean Sci. Discuss., 3, 435–470, 2006
www.ocean-sci-discuss.net/3/435/2006/

Ocean Science Discussions

Papers published in *Ocean Science Discussions* are under open-access review for the journal *Ocean Science*

Improved near real time surface wind resolution over the Mediterranean Sea

A. Bentamy, H.-L. Ayina, P. Queffeulou, and D. Croize-Fillon

Institut Français pour la Rechercher et l'exploitation de la MER (IFREMER), DOPS, BP 70, 20280 Plouzane, France

Received: 24 March 2006 – Accepted: 28 April 2006 – Published: 13 June 2006

Correspondence to: A. Bentamy (abderrahim.bentamy@ifremer.fr)

Abstract

Several scientific programs, including the Mediterranean Forecasting System Toward Environmental Predictions (MFSTEP project), request high space and time resolutions of surface wind speed and direction. The purpose of this paper is to focus on surface wind improvements over the global Mediterranean Sea, based on the blending near real time remotely sensed wind observations and ECMWF wind analysis. Ocean surface wind observations are retrieved from QuikSCAT scatterometer and from SSM/I radiometers available at near real time at Météo-France. Using synchronous satellite data, the number of remotely sensed data available for each analysis epoch (00:00 h; 06:00 h; 12:00 h; 18:00 h) is not uniformly distributed as a function of space and time. On average two satellite wind observations are available for each analysis time period. The analysis is performed by optimum interpolation (OI) based on the kriging approach. The needed covariance matrixes are estimated from the satellite wind speed, zonal and meridional component observations. The quality of the 6-hourly resulting blended wind fields on 0.25° grid are investigated trough comparisons with the remotely sensed observations as well as with moored buoy wind averaged wind estimates. The blended wind data and remotely wind observations, occurring within 3 h and 0.25° from the analysis estimates, compare well over the global basin as well as over the sub-basins. The correlation coefficients exceed 0.95 while the rms difference values are less than 0.30 m/s. Using measurements from moored buoys, the high-resolution wind fields are found to have similar accuracy as satellite wind retrievals. Blended wind estimates exhibit better comparisons with buoy moored in open sea than near shore.

1 Introduction

Several processes related to off-shore activities require the knowledge of accurate surface winds and sea states on fine high space and time resolution. The former are both critical for determining the dynamical forcing of the ocean, the estimation of ocean

OSD

3, 435–470, 2006

surface currents, waves and related boundary layer processes, and the dispersion and drift of oil and other pollutants. This is particularly true for the Mediterranean sea, which is one largest enclosed sea basin in the world. It spans from 30° N to 48° N in latitude, and from 5° W to 37° E. Its geometry is quite complicated and characterized by the extended mountains on its border and by the presence of several islands. The slopes are often rapidly diving from mountain tops to sea level. It has mainly two consequences on the wind flows. Firstly, it creates coastal turbulences. The presence of big islands (Corsica, Sardinia, Sicily, Crete...) dramatically disrupts the air flows in their vicinity. The second effect of near coast orography is breezes blowing alternatively from land or from sea. This semi diurnal phenomenon is essentially linked to heat, and has hence a greater effect during the summer. The complicated geometry, orography, and meteorology may have a great impact on the accuracy of the surface parameters (Komen et al., 1994). Among the main surface parameters involved in the atmosphere-ocean exchange are the surface wind and the related momentum flux (wind stress and curl). They are routinely provided in near real time by the European National Meteorological Services (NMSs) as well as by the European Centre for Medium range Weather Forecast (ECMWF). The surface winds are also estimated from radars and radiometers onboard satellites and their assimilation allows significant improvement of forecast and analysis NWP products (see for instance Crapolicchio et al., 1995). However, the spatial resolution of the operational numerical wind model is smoothed and several fine resolutions of about 25 km–100 km, requested by wave and oceanic models or by process studies (Queffeulou, 2005), are missed (Chen, 2003).

Over the Mediterranean sea, the surface wind vector is characterized by a large spatial and temporal variability. Even though the seasonal signal is quite common to several sub-basins of the Mediterranean sea, significant regional changes in its amplitude and phase are depicted (Bentamy et al., 2005). Indeed, several local wind conditions exist (Brody et al., 1980) and might have remotely impact on the global space and time wind patterns. For instance, some large scale wind regimes have been identified and documented. The Mistral wind flows into Gulf of Lion from the southern coast of France.

The Etesian flows mostly in the Aegean Sea and into the eastern Mediterranean. Bora is a north to northeast wind flowing in the Adriatic sea. Sirocco, southeast to southwest wind, blows from Libya and Egypt coasts toward north into the south-central Mediterranean sea. There are two major winds flowing in the Alboran Channel and through the Strait of Gibraltar : Westerly and Levante winds (east to northeast). Using about ten years of remotely sensed wind speed and direction (Bentamy et al., 2002), it is stated that the highest wind conditions are located in Mistral and Etesian regions. Most of Mistral and Etesian wind conditions (determined according to their climatological patterns) are characterized by wind speed higher than 11 m/s. Their occurrence number during winter season (December, January, February) is about 70% higher than summer's.

To meet the Mediterranean Forecasting System Toward Environmental Predictions (MFSTEP project) requirements, high space and time resolutions of surface wind speed and direction are estimated from merging ECMWF operational wind analyses and near real time remotely sensed wind observations. The resulting wind fields will be indicated as the blended near real time wind products. The improvement of surface wind resolution as well as accuracy is also articulated by several international programs (e.g. WCRP, http://www.wmo.ch/web/wcrp/wcrp-home.html, AMMA http://amma.mediasfrance.org, MERSEA, http://www.mersea.eu.org/).

In this study, the surface wind retrievals are derived from SeaWinds scatterometer onboard QuikScat, and from the Special Sensor Microwave Imager (SSM/I) onboard the Defense Meteorological Satellite Program (DMSP). Previous studies have been carried out to estimate the accuracy of the off line satellite surface wind through comparisons to in-situ and/or numerical model estimates (e.g. Boutin et al., 1999; Meissner et al., 2001, Bentamy et al., 2002; Ebuchi et al., 2002; Bourassa et al., 2003). For instance, the comparison of moored buoy wind measurements and off-line QuikScat wind observations indicates that the remotely sensed winds compare well with in-situ measurements. The rms differences of wind speed and direction are about 1 m/s and 23°, respectively, while the correlations exceed 0.86. Quite similar results are found for SSM/I off line wind estimates. The off-line satellite data are then used to investigate

the quality of near real time satellite data over the Mediterranean Sea.

The paper is organized as follows: Section 2 describes the data used in this study with general statistics. The objective method allowing the calculation of the blended wind fields is presented in Sect. 2. The validation and the spatial and temporal patterns of the blended wind speed and direction are examined in Sect. 4. Finally, a summary with conclusions are presented in Sect. 5.

2 DATA

2.1 Scatterometer

The scatterometer principle is described in wide scientific and technical papers (see for instance JPL, 2001). The scatterometer antennas emit towards surface microwaves, which are scattered by short sea waves (capillary/gravity waves). The latter are strongly related to changes in surface winds. The fraction of transmitted power that returns to the satellite, called backscatter coefficient (σ°), is a function of wind speed and direction.

More specifically, QuikScat/SeaWinds has a rotating antenna with two differently polarized emitters: the H-pol with incidence angle of 46.25° and V-pol with incidence angle of 54°. The inner beam has a swath of about 1400 km, while the outer beam swath is 1800 km width. The spatial resolution of SeaWinds σ° (oval footprint) is of 25×35 km. The latter are binned over the scatterometer swath into cells of 25×25 km, called Wind Vector Cell (WVC). There are 76 WVC across the satellite swath, and each contains the center of 10 to 25 measured σ°. The remotely wind vectors are estimated from the scatterometer σ° over each WVC using the empirical model QSCAT-1 relating the measured backscatter coefficients to surface winds. Every day, about 1.1 million 25-km ocean surface wind vector observations are retrieved from QuikScat measurements covering about 90% of the Earth surface.

Even though, the study concerns near real time issues, two QuikScat data sources

OSD
3, 435–470, 2006

EGU

are used. The first one is generated in near real time by National Oceanic and Atmospheric Administration (NOAA/NESDIS: http://manati.orbit.nesdis.noaa.gov), while the second one is generated and provided in off-line time by Jet Propultion Laboratory (JPL: http://podaac.jpl.nasa.gov/). The study includes data from L2A product, related to backscatter measurements, and from L2B product related to wind vector retrievals. One main difference between NRT and off-line QuikScat products is the spatial resolution of the backscatter coefficient (σ°). In NRT products, σ° is an average of all backscatter coefficients measured by the same beam (fore-inner, fore-outer, aft-inner, aft-outer) and located within a given WVC. In off-line product, each σ° is given at its nominal spatial resolution. Both L2B products have been calculated using the standard scatterometer method based on the Maximum Likelihood Estimator (MLE) (JPL, 2001). The scatterometer retrieval algorithm estimates several wind solutions for each wind cell. In general speaking there are four solutions. The ambiguity removal method is then used to select the most probable wind solution. The latter are used in this study. To improve the wind direction, especially in the middle of swath where the azimuth diversity is quite poor, an algorithm called Direction Interval Retrieval with Threshold Nudging (DIRTH) is used too.

SeaWinds is a Ku band radar. Therefore, rain has a substantial influence on its measurements. Previous studies (Sobieski et al., 1999) showed that the rain impact may attenuate the scatterometer signal, resulting in wind speed underestimation, or change the surface shape due to raindrop, allowing an overestimation in the retrieved winds. The QuikScat wind products involve several rain flag determined from the scatterometer observations and from the collocated radiometer rain rate onboard other satellites.

For each QuikScat orbit, NRT and Off-line L2A and L2B data are collocated in space within the same wind vector cell (WVC). It was found (not shown) that both backscatter coefficients σ° compare well. The mean bias is about 0.05 dB and is not statistically significant. The rms value is about 1.10 dB and is related to the collocation procedure. Indeed, for each WVC, the number of NRT composite sigma0 cannot exceed 4, while the number of L2A (egg) sigma0 may reach 32. The main discrepancies are found for

low σ° values related to low surface winds. Excluding these low values reduces the rms of H-pol and of V-pol σ° differences to 0.80 dB and 0.66 dB, respectively.

NRT and Off-line wind products provide two wind speed and direction types. The first one is the standard wind data, which have been processed using the Maximum Likelihood Estimator (MLE) method (Long et al., 1991) and median filter ambiguity removal algorithm with the Numerical Weather Prediction data. The second is enhanced wind data processed using the Direction Interval Retrieval with Thresholeded Nudging (DIRTH) algorithm (JPL, 2001). The comparison between Off-line and NRT wind retrievals does not indicate any systematic bias in wind speed or direction. The bias and rms of wind speed and of wind direction differences are quite small. However, some high discrepancies are depicted in wind direction comparison. They are mainly related to wind speed less than 5 m/s. Excluding these surface wind conditions, the rms difference of wind direction drops to 6°. Further investigations have been performed to characterize the wind speed and wind direction differences as a function of some parameters, such azimuth angle, WVC index, longitude, and latitude. No significant dependencies have been found. The impact of rain contamination is more significant. Indeed, more than 17% of WVC are indicated rain free for NRT wind data, while for off-line wind data, they are indicated rain contaminated. Using only the rain flag provided with NRT wind data increases the rms wind speed difference by about 30%.

To improve rain detection in QuikScat NRT data, the method developed by Portabella et al. (2002), based on the use of MLE estimation calculated from NRT σ°, is implemented to determine a new NRT rain flag (called hereafter KNMI rain flag). The former impact is investigated trough the comparison between available off-line and NRT data both estimated over the same WVC and orbit. Three cases of rain free NRT wind data are considered. They are associated to the use of NRT rain flag, combination of NRT and off-line rain flags, and combination of NRT and KNMI rain flags, respectively. Table 1 summarizes the main statistical parameters characterizing the comparisons of off-line and NRT wind speeds and directions during January 2004, and over the Mediterranean Sea. The difference between off-line and NRT wind estimates is low.

However, the use of the combination of NRT and KNMI rain flag provides a slight improvement in terms of wind speed as well as in wind direction comparisons. The main impact of KNMI rain flag is found for the high values of off-line and NRT wind difference. Indeed, the number of differences exceeding two times standard deviation of the overall difference (0.74 m/s) is reduced by a factor 49% in the third case. Furthermore, the 95% percentile of the differences calculated for the three cases is about 1.19 m/s, 0.87 m/s, and 0.97 m/s respectively.

2.2 Radiometers

The SSM/I radiometers onboard the DMSP F13, F14, and F15 satellites provide measurements of the surface brightness temperatures at frequencies of 19.35, 22.235, 37, and 85 GHz (hereafter referred to as 19, 22, 37, and 85 GHz), respectively. Horizontal and vertical polarization measurements are taken at 19, 37, and 85 GHz. Only vertical polarization is available from 22 GHz. Due to the choice of the channels operating at frequencies outside strong absorption lines [for water vapor] (50–70 GHz), the radiation measured by the antennae is a mixture of radiation emitted by clouds, water vapor in the air and the sea surface, as well as radiation emitted by the atmosphere and reflected at the sea surface. For the estimation of the 10-m wind speed from SSM/I brightness temperatures, the algorithm published by Bentamy et al. (1999) is used. The latter is a slightly modified version Goodberlet et al. (1989) algorithm and includes a water vapor content correction. The SSM/I wind speeds are calculated over swaths of 1394-km width, with a spatial resolution of 25 km×25 km. The retrieved wind speed was calculated from brightness temperature measurements provided by NASA Marshall Space Flight Center (MSFC). Previous studies investigated the accuracies of the retrieved SSM/I winds through comparisons with moored buoy wind measurements in several oceanic regions (Bentamy et al., 2002). The standard error values of SSM/I wind speeds with respect to the buoy winds are less than 2 m/s. The bias values do not exceed 0.20 m/s.

The NRT brightness temperatures as well as retrieval winds were compared to

MSFC data. No significant differences were found. Furthermore, the NRT winds are compared to Remote Sensing System (http://www.remss.com) data too. The latter were used and validated by several authors in various oceanic regions (see for instance Meissner et al., 2001). NRT and RSS swath wind data are collected over the Atlantic ocean and the Mediterranean sea ocean during January 2004. Only validated wind data (about 3 900 000 for NRT and 4 200 000 for RSS), based on quality control related to each wind source, are used. The main result are RSS and NRT data present an almost identical distribution especially for wind speed laying between 3 and 18 m/s (more than 90% of total data): NRT and RSS provide quite similar winds with close mean and standard deviation values. The Student's test, estimating the statistical significance between two mean values, indicates that SSM/I NRT and RSS means are the same with 95% confidence. The main discrepancy between the two sources is found out for high winds. More than 2.5% of RSS wind data exceed 18 m/s whereas they are only 0.1% for NRT. Most of cases of high surface winds and significant difference between RSS and NRT are related to rain detection. In NRT, the rain flag seems rejecting several high wind estimates.

3 Objective method

The method aims to estimate gridded wind fields from ECMWF operational surface wind analysis and from near real time satellite surface parameter observations, at regular space and time resolutions. The method is based on the kriging approach analyzing the differences between ECMWF data and satellite observations.

3.1 Numerical procedure

Let us assume that:

$$X_a = \tilde{X} + \varepsilon_a \text{ and } X_a = \tilde{X} + \varepsilon_b \quad (1)$$

where X_a is the expected analysis value estimated at grid point of δh degree in longitude and latitude and over δt hours. Three spatial resolutions δh are considered: 0.25°, 0.5°, and 1°, while the temporal resolutions δt are: 6 h, 12 h, and 24 h.

X_b stands for background vector (from ECMWF) available every 6 h and over grid point of 0.5° degrees in longitude and latitude at global ocean. For δh of 0.25°, ECMWF analysis are linearly interpolated. For δh of 1°, ECMWF data are averaged over the grid point.

$\tilde{X}$ is the true surface surface parameter, while ε_a, ε_b are the associated errors to X_a and to X_b, respectively.

Therefore $X_a = X_b + \tilde{\varepsilon}$. Where $\tilde{\varepsilon}$ is a combination of ε_a and ε_b. Its values are estimated from remotely sensed observations as follows:

$$\hat{\varepsilon}_i = \frac{1}{(t_b - t_a)} \int_{ta}^{tb} \left(\sum_{j=1}^{N} \lambda_j \left(X_o^j \left(x_j, y_j, t \right) - X_{bo}^j \left(x_j, y_j, t \right) \right) \right) dt \tag{2}$$

$\hat{\varepsilon}_i$ stands for $\tilde{\varepsilon}$ estimator at grid point M_i over the period $\delta t = t_b - t_a$.

X_{bo}^j is the jth background surface parameter interpolated in space and time over satellite swath.

X_o^j indicates the jth remotely sensed observation vector available over satellite swath.

$(X_o^j - X_{bo}^j)$ jth difference between satellite observation and ECMWF analysis located in space and time neighborhood of grid point $M_i = (x_i, y_i, t_i) \cdot x_i, y_i$ state for longitude and latitude while t_i is the time.

λ is the weighting vector to be estimate. Its determination, at each grid point, leads to minimize the residual

$$R = \tilde{\varepsilon} - \hat{\varepsilon} \text{ with the unbiased constraint } \sum_{j=1}^{N} \lambda_j = 1 \tag{3}$$

The Gauss Markov theorem indicates that the best estimator in the least-square optimum linear estimator should minimize $\mathrm{Var}(R)=E((\tilde{\varepsilon}-\hat{\varepsilon})^2)$. Operator E states for mathematical mean.

At a given grid point $M_0=(x_0, y_0, t_0)$ (x_0, y_0, t_0 indicate geographical coordinates and time)

$$\mathrm{Var}\left(R\left(M_0\right)\right) = \mathrm{Var}\left(\tilde{\varepsilon}\left(M_0\right)\right) + \mathrm{Var}\left(\hat{\varepsilon}\left(M_0\right)\right) - 2\mathrm{Cov}\left(\tilde{\varepsilon}\left(M_0\right), \hat{\varepsilon}\left(M_0\right)\right) \quad (4)$$

Cov indicates the covariance.

$$\mathrm{Var}\left(\hat{\varepsilon}\left(M_0\right)\right) = \mathrm{Var}\left(\sum_{j=1}^{j=N} \lambda_j \left(X_o^j - X_{bo}^j\right)\right) = E\left(\sum_{j=1}^{j=N} \lambda_j \left(X_o^j - X_{bo}^j\right)\right)^2 - \left(\sum_{j=1}^{j=N} \lambda j E\left(X_o^j - X_{bo}^j\right)\right)^2 \quad (5)$$

$$\mathrm{Var}\left(\hat{\varepsilon}\left(M_0\right)\right) = \sum_{j=1}^{j=N}\sum_{l=1}^{l=N} \lambda_j\lambda_l E\left(\left(X_o^j - X_{bo}^j\right)\left(X_o^l - X_{bo}^l\right)\right) - \left(\sum_{j=1}^{j=N} \lambda_j E\left(X_o^j - X_{bo}^j\right)\right)^2 \quad (6)$$

Assuming that the difference between observation and analysis is homogeneous over M_0 neighborhood (first intrinsic assumption) :

$$E\left(X_o^j - X_{bo}^j\right) = E\left(X_o^l - X_{bo}^l\right) = m \quad (7)$$

This assumption states that the mean of difference between observation and analysis is independent of space and time separation. To assess such assumption, one month of interpolated ECMWF and QuikScat 10 m winds are used. Three temporal separations between the two sources are considered: 6 h, 12 h, and 24 h. The investigation is performed in boxes of 5° in longitude and latitude over the Mediterranean Sea. Over each box and for each separation time, the mean value of difference $\tilde{\varepsilon}(M_i)-\tilde{\varepsilon}(M_j)$ is estimated as a function of spatial distance between M_i and M_j for wind speed, zonal, and meridional components. It is found (not shown) that the mean values of $\tilde{\varepsilon}(M_i)-\tilde{\varepsilon}(M_j)$

OSD
3, 435–470, 2006

EGU

are very small and do not exceed 0.03 m/s. Student's test establishes the mean values are not statistically different from 0.

Therefore Eq. (7) leads to

$$\mathrm{Var}\left(\hat{\varepsilon}\left(x0\right)\right) = \sum_{j=1}^{j=N}\sum_{l=1}^{l=N}\lambda_j\lambda_l E\left(\left(X_o^j - X_{bo}^j\right)\left(X_o^l - X_{bo}^l\right)\right) - \sum_{j=1}^{j=N}\sum_{l=1}^{l=N}\lambda_j\lambda_l m^2$$

$$\mathrm{Var}\left(\hat{\varepsilon}\left(M0\right)\right) = \sum_{j=1}^{j=N}\sum_{l=1}^{l=N}\lambda_j\lambda_l \mathrm{Cov}\left(\left(X_o^j - X_{bo}^j\right), \left(X_o^l - X_{bo}^l\right)\right) \quad (8)$$

Furthermore

$$\mathrm{Cov}\left(\tilde{\varepsilon}\left(M_0\right), \hat{\varepsilon}\left(M_0\right)\right) = E\left(\sum_{j=1}^{j=N}\lambda j\left(X_o^j - X_{bo}^j\right)\right)\left(X_o^0 - X_{bo}^0\right) - m^2$$

$$= \sum_{j=1}^{j=N}\lambda j \mathrm{Cov}\left(\left(X_o^j - X_{bo}^j\right), \left(X_o^0 - X_{bo}^0\right)\right) \quad (9)$$

Therefore, using Eqs. (3), (8), and (9):

$$\mathrm{Var}\left(R\left(M_0\right)\right) = \mathrm{Var}\left(\tilde{\varepsilon}\left(M_0\right)\right) + \sum_{j=1}^{j=N}\sum_{l=1}^{l=N}\lambda_j\lambda_l\hat{C}_{ij} - 2\sum_{j=1}^{j=N}\lambda_j\hat{C}_{i0} \quad (10)$$

where $\hat{C}_{ij}$=Cov($\hat{\varepsilon}(M_i)$, $\hat{\varepsilon}(M_j)$).

Minimizing functional Var($R(M_0)$) in weighting space and under unbiased constraint leads to the following linear system:

$$\begin{cases} \sum_{j=1}^{j=N}\lambda_j\hat{C}_{ij} - \mu = \hat{C}_{i0} \text{ for } i = 1, N \\ \sum_{j=1}^{j=N}\lambda_j = 1 \end{cases} \quad (11)$$

μ is the Lagragian term used to take into account the unbiased constraint.

3.2 Space and time structure

The objective method requires parameterization of the spatial and temporal covariance structure of the difference between remotely sensed wind and the background NWP data. The approach used in Bentamy et al. (1996) is adapted for this study. First, the local spatial and temporal stationarity is assumed. Therefore, the covariance does not depend on the precise geographical location and epoch of data, but only on the separation in space and time.

$$\mathrm{Cov}\left(\tilde{\varepsilon}\left(M_i, t_i\right), \varepsilon\left(M_j, t_j\right)\right) = C\left(\delta h, \delta t\right) \tag{12}$$

where δh and δt stand for spatial and temporal separation, respectively.

As the assessment of this assumption is not straightforward, the following assumption is considered:

$$E\left(\tilde{\varepsilon}\left(M_i, t_i\right) - \tilde{\varepsilon}\left(M_j, t_j\right)^2\right) = G\left(\delta h, \delta t\right) \tag{13}$$

Using the first intrinsic assumption (Eq. 7) :

$$G\left(\delta h, \delta t\right) = 2\left(C\left(0, 0\right) - C\left(\delta h, \delta t\right)\right) \tag{14}$$

In practice, the following structure function, called variogram, is used

$$\Gamma\left(\delta h, \delta t\right) = C\left(0, 0\right) - C\left(\delta h, \delta t\right) \tag{15}$$

The objective is to determine covariance matrix involving the main spatial and temporal structure of variable $\tilde{\varepsilon}$ without any prior gridding or spectral filtering. Therefore, the investigation of covariance or variogram behavior as a function of space and time separation is performed at several areas of the Mediterranean sea. To calculate the sample covariance, the spatial and temporal collocated QuikScat and ECMWF wind data are used. The observed values of $\tilde{\varepsilon}$ are then calculated over each satellite WVC

OSD
3, 435–470, 2006

EGU

and stratified in terms of 1-hourly time windows (WVC time). Figure 1 shows an example of wind speed ($\tilde{\varepsilon}_w$) variogram behaviors as a function of spatial separation for lag time less than one hour. They are estimated for winter and summer seasons over three 5° boxes centered at 4° E–42° N, 19° E–36° N, and 29° E–33° N, respectively. As expected, the variogram increases with respect to increasing separation, notifying that correlation decreases with increasing spatial separation. The variogram estimations from observations exhibit high spread for all separation ranges mainly related to the high variability of $\tilde{\varepsilon}$ variable. Consequently, the parameterization of covariance matrix should tack into account such variation. Furthermore, the former should ensure that the covariance matrix is positive-definite. Several formulations of positive-definite analytical function dealing with the empirical variogram fitting exist and are commonly used. In this study the following formulation is used:

$$\hat{\Gamma}(\delta h, \delta t) = \varepsilon_p + a\left(1 - \exp\left(-\frac{\delta h + c\delta t}{b}\right)\right) \tag{16}$$

ε_p, a, b, c are the variogram model parameters.

ε_p stands for $\tilde{\varepsilon}$ noise. b and c are the spatial and temporal characteristic decorrelation scales, respectively. Parameter a, named sill value, indicates the variogram value reached for spatial and temporal ranges where variables are uncorrelated.

The variogram parameters are estimated as minimum solution of:

$$F\left(\varepsilon_p, a, b, c\right) = \left(\frac{\Gamma(\delta h, \delta t) - \hat{\Gamma}(\delta h, \delta t)}{\sigma(\delta h, \delta t)}\right)^2 \tag{17}$$

$\sigma^2(\delta h, \delta t)$ indicates the variance of the observed variogram.

The parameters are determined over several Mediterranean sub-basins using remotely sensed and ECMWF wind differences during winter and summer season (north hemisphere). Table 2 provides a, b, and c estimates and their accuracies in terms of 95 confidence intervals. ε_p is found small and remains nearly constant as a function of geographical area as well as a function of period. The variogram parameter a, b, and

c changes are significant with respect to geographical area and season. The highest spatial and temporal decorralation length (b) values are found.

4 Accuracy of blended fields

The previous method is used to estimate the gridded wind fields over the Mediterranean sea. Even though several space and time resolutions are investigated, this section is focused on the derived wind fields with the spatial resolution of 0.25° in longitude and latitude, and temporal resolution of 6 h. The quality of the resulting near real time blended wind fields is investigated trough several comparisons over the global basin as well as at some specific locations.

4.1 Global analysis

To evaluate the quality of the previous method, surface wind fields are calculated from near real time satellite and ECMWF winds. For each ECMWF wind analysis available at synoptic time (00:00 h; 06:00 h; 12:00 h; 18:00 h) all valid satellite data (scatterometer, radiometers) available within 3 h from ECMWF time are selected. An interpolation method is used to estimate ECMWF winds over each satellite wind cells:

$$X_{\mathrm{bo}} = \frac{1}{\sum_{i=1}^{i=N} \frac{1}{di}} \sum_{i=1}^{i=N} \left(\frac{1}{di} X_b \right) \tag{18}$$

di is the spatial separation between satellite wind cell and ith ECMWF grid point.

The quality of the blended wind fields is mainly related to the accuracy of the remotely sensed data accuracy and to the spatial and temporal sampling scheme of the observations. Using all validated QuikScat and SSMI (F13, F14, and F15) retrieval winds, we can expect (on average) two observations within each grid point (0.25°×0.25°) and within 3 h from ECMWF synoptic time. However, this number varies according to space

and time. For instance, in western area (6° W–10° E) the mean number of satellite observations exceeds 3 for 12:00 h time analysis. Figure 2 illustrates such issue at a specific location. It shows the number of satellite observations during January 2004. It indicates that the observation length is not same for the four synoptic time analysis. Furthermore, the sampling satellite wind observations is not uniform over the whole basin. Indeed, in open sea areas the number of satellite observations falling within each grid point (0.25° resolution) and result for each epoch (6 h) is on average 3. This number drops to less than 1 in nearshore areas and in the Aegean sea. The impact of the satellite sampling scheme is investigated using the method previously published by several authors (e.g. Mestas et al., 1994; Bentamy et al., 1998). Briefly, in Eq. (7) the validated satellite observation is replaced by the nearest, in space and time, ECMWF analysis. The resulting wind fields are then compared to the 6-hourly operational ECMWF analyses during January 2004 and over the Mediterranean Sea. The overall statistics characterizing the difference between the two wind fields indicate that the bias and the standard deviation are quite small and do not exceed 0.50 m/s for wind speed as well as for wind components. The correlation between the two fields is very high and about 0.99. However, some high local differences are depicted. For instance in Mistral track, characterized by high and variable surface winds, the difference at some grid point reaches 1 m/s related to the smoothing of ECMWF winds used as observation and background, and to the satellite sampling schemes.

The longitude, latitude, and time of the satellite wind cell are associated to the variable $\tilde{\varepsilon}=X_o-X_{bo}$. A typical spatial distribution of $\tilde{\varepsilon}$ observations is shown in Fig. 3. It exhibits an interesting sampling length over the oceanic basin. However, high spatial variability is clearly depicted and provides an illustration of spatial and temporal structure function results obtained in previous section.

For this study, the $\tilde{\varepsilon}$ observations are derived from QuikScat-ECMWF (wind speed, zonal and meridional components) and from F13, F14, and F15 SSM/I-ECMWF (wind speed). At each SSM/I wind cell, the wind direction is derived from the interpolated ECMWF analysis. The objective method is used to analysis $\tilde{\varepsilon}$ over global ocean with

a spatial resolution of 0.25 in longitude and latitude, and with temporal resolution of 6 h (00:00 h, 06:00 h, 12:00 h, 18:00 h). For given epoch, $\tilde{\varepsilon}$ observations are stratified in hourly time intervals and at each grid point, and data related to QuikScat are first selected to be used in the analysis. Figure 4 illustrates an example of blended method result. It shows ECMWF wind field analysis of 2 January 2004 at 12:00 h (Fig. 4a) and the corresponding blended wind product (Fig. 4b), remotely sensed wind observations (Fig. 4c), and satellite – ECMWF winds (Fig. 4d). As expected, the Figure shows that blended wind data are close to satellite retrieved winds and most of biases (Fig. 4d) are removed. This result is confirmed by the investigation of blended wind product consistency during January 2004 and at various Mediterranean sub-basins. Table 3 summarizes the comparisons between satellite wind observations and blended data. The latter are interpolated over satellite swaths (Eq. 18). Results related to satellite observation and ECMWF analysis comparisons are shown too. On average, the bias between satellite observation and blended wind analysis is very low. The RMS values do not exceed 0.30 m/s. As seen from Table 3 both the pattern and the amplitude of the numerical analysis winds agree quite well with those derived from satellite measurements. The statistics related to the satellite and ECMWF comparisons are quite similar to those obtained over the global ocean (Monahan, 2006) indicating an overestimation of remotely sensed winds compared to ECMWF analysis. Although not shown, this agreement is particularly good within the regions off coasts. The main discrepancies are found in near coasts areas. In the latter areas remotely sensed wind observations (mostly from QuikScat) are up to 2 m/s stronger and has a weaker onshore component. Such discrepancies may be related to the accuracy of satellite retrievals near shore areas (Picket et al., 2003), and to the spatial smoothing used in the numerical analysis and the related spatial resolution. The comparisons between blended wind product and ECMWF analysis exhibit quite similar patterns than satellite and ECMWF. The mean and the standard deviation of the difference between blended and ECMWF wind speed, calculated over the whole Mediterranean sea and during January 2004, are about 1.03 m/s and 1.50 m/s, respectively. The highest discrepancies between the

two wind sources is located in neareshore and Aegean sea, might be related to the poor satellite sampling.

4.2 Comparison with buoy measurements

The quality of the blended wind products is primarily investigated through comparisons with wind speeds and directions measured by moored buoys in the Mediterranean sea. However to enhance the comparison quality, some moored buoy in the Atlantic areas, close to the Mediterranean sea, are used too. The buoys are provided by Météo-France and Puertos del Estado in Spain. Table 4 indicates the buoy positions. Except buoy 62001, the buoy locations are ranged between 8 to 120 km off coast. Only buoys providing significant sampling length (more than 15 days) of wind measurements are used in these comparisons. Even though the buoy data are already assimilated in ECMWF analysis, they provide valuable method to assess the quality and especially the temporal characteristics of the blended. Buoys supply hourly oceanic and atmospheric data. 10 m buoy winds are calculated from raw data and 6-hourly averaged. The buoy data are collocated in space and time with ECMWF and blended winds as well as with remotely sensed wind observations. Table 5 shows statistics derived from all available buoy and blended, ECMWF, QuikScat, and SSM/I wind data. Even tough the sampling length is small yielding to less meaning of the statistical parameters, some obvious results may point out. As expected and due to the assimilation of buoy in ECMWF analysis, buoy and ECMWF comparisons exhibit the highest correlation and the lowest standard deviation difference values. Blended winds exhibit quite similar statistics than QuikScat and SSM/I observations. Their correlations with buoy winds are high and exceed 0.80, while the bias values indicate a slight overestimation of blended wind speed estimates (about 40 m/s in the Mediterranean sea, and 0.30 m/s in the Atlantic basin). The statistics estimated at the Mediterranean and the Atlantic sites do not indicate significant difference, especially in wind speed. Indeed, using fischer test, the difference between the Mediterranean and the Atlantic correlation coefficients is not significant with 95% confidence. The differences are found in wind directions (zonal and merid-

ional components) related to the orography impact and to the wind distribution. Indeed, about 25% of the Mediterranean buoy winds are lower than 4 m/s, while in the Atlantic, the percentage is about 15%. Excluding buoy winds lower than 4 m/s yields to similar statistics in both ocean areas.

The differences between 6-hourly averaged buoy and blended winds involve the satellite sampling schemes discussed in the previous section. Indeed, in the vicinity (spatial distance less than 25 km) of the two off-shore Mediterranean buoys 61001 and 61002 (Table 4) , on average three satellite wind observations are expected within a given epoch (Fig. 2). Most of the observations occurred between 03:00 a.m. and 09:00 a.m., and between 03:00 p.m. and 09:00 p.m. To investigate the impact of such sampling on the statistics characterizing the difference between buoy and blended wind data (Table 5), the hourly buoy data occurring half hour from satellite observations and three hours from synoptic time (00:00 h, 06:00 h, 12:00 h, 18:00 h) are collected and averaged. They are called simulated buoy data. The latter are compared to the 6-hourly averaged buoy data use to estimate the accuracy of blended wind estimates. During January 2004, the rms difference between 6-hourly averaged buoy and simulated buoy wind speed, zonal component, and meridional component are 1.20 m/s, 1.14 m/s, and 1.29 m/s, respectively for 61001 buoy. For buoy 61002, these quantities are 1.02 m/s, 1.00 m/s, and 1.10 m/s, respectively. These examples illustrate that the rms differences between buoy and blended data are a combination of several errors related to the difference between buoy measurements and remotely sensed wind observations, to the sampling scheme issue, and to the objective method.

Even though some significant buoy-to-buoy differences are found, the blended wind estimates capture the main wind temporal patterns at each buoy position. For instance, Figs. 5–7 show time series of wind speed, zonal wind component, and meridional components from blended (heavy line), ECMWF (dashed line), and from 61001, 61002, and 2 029 012 buoys (light line), respectively. They illustrate the good agreement between the three sources, and indicate that the main fast wind changes as well as the high wind conditions measured by buoys are retrieved by blended. Indeed, considering only

wind speeds higher than third percentile estimated from buoy measurements , allows another insight in comparison results. In the Mediterranean sea and during January 2004, the buoy wind speed third percentile is 10.28 m/s. The percentage of blended winds exceeding this percentile is 26%, while for ECMWF is 18%. Such results indicate that high wind condition, generally associated with high spatial and temporal variation, are well retrieved.

5 Summary and conclusions

A method was presented, validated, and used to estimate one month of gridded wind fields over the Mediterranean sea with high spatial and temporal resolution. It is mainly based on the use of several remotely sensed surface winds (wind speed, zonal and meridional components), derived from scatterometer onboard QuikSCAT satellite, and SSM/I radiometers on board DMSP F13, F14, and 15 satellites, in combination with winds from the operational ECMWF analysis available at synoptic time. The two kinds of wind sources were blended through the objective analysis of their differences, calculated over each individual satellite swath, based on the kriging approach. The requested wind speed, zonal and meriodional variograms were estimated from the observed ECMWF-QuikSCAT wind differences. It was shown that the main parameters characterizing their behaviors as a function of spatial and temporal separations may change according to sub-basin. As blended wind fields were only estimated for January 2004, the empirical variogram determined during winter season was used. Further refinements will be attempted in order to include the seasonal and regional variogram behavior. However, the impact of the variogram on the blended error is lower than the accuracy of each remotely sensed wind and the satellite instrument sampling scheme. Indeed, the use of near real time retrieval scatterometer and radiometer winds requested validation issues. They were performed through comparisons to the associated off-line winds. The main results are the adaptation of KNMI rain flag for QuikSCAT winds and the correction of SSM/I winds using an empirical model based

on the collocation of QuikSCAT and SSM/I winds at global ocean. Furthermore, this study indicates that the quality of blended wind vector fields strongly depends on the satellite observation time. The simulation of the impact of such time sampling was investigated using buoy data and indicated for instance that the wind speed error may exceed 1 m/s. The resulting blended wind fields were verified by comparison with the satellite wind observations as well with buoy measurements several Mediterranean sea location, including nearshore buoys. As buoy data are assimilated in ECMWF analysis, they cannot be considered independent. As expected, blended and averaged satellite wind observation exhibit very high correlation coefficients (about 0.99) and very low biases. The agreement between blended and the 6-hourly averaged buoy wind estimates is good. The correlation coefficients are quite high (exceeding 0.85) . The statistical parameters characterizing the differences between buoy and blended data are quite similar to those obtained from buoy and satellite comparisons. However, the data set of this study is quite small yielding to less significant of the statistical parameters. The latter found in this study are highly related to the atmosphere and oceanic conditions during January 2004. Furthermore, the use of a small collocated data emphasizes the main problem related to the comparison of moored buoy to satellite data: Satellite data are asynoptic and have complex swath based spatial coverage patterns, while buoy sampling is 8 min averaging on the hour and the derived wind vector is strongly related to the local wind condition. Therefore, to assess the quality of the near real time blended wind fields, longer (more than 3 years) time series are obviously needed and recommended.

In the future, more satellite wind data will be involved in the blended analysis. Indeed, since 2003 the experiment satellite Windsat provides an estimation of ocean vector winds from polarimetric microwave radiometers. Next June 2006, the satellite METOP will be launched with a new scatterometer onboard providing surface winds with a spatial resolution of $0.25^{\circ} \times 0.25^{\circ}$. In parallel, the accuracy of the blended long time series will be investigated through their impact in a oceanic circulation model forcing experiments.

Acknowledgements. This study was funded by Mediterranean Forecasting Towards Environmental Predictions (MFSTEP) and by Marine and EnviRonment and Security for European Area (MERSEA) European integrated projects. We thank CERSAT and Météo-France teams for help with processing the raw satellite near real time data. We are grateful to the institutes that maintain buoy networks and make available high quality surface parameters estimates (Météo – France; UK Met Office, EPEE).

References

Bauer, E.: Characteristic frequency distributions of remotely sensed in situ and modeled wind speeds, Int. J. Climatol., 16, 1087–1102, 1996.

Bentamy, A., Grima, N., and Quilfen, Y.: Validation of the gridded weekly and monthly wind fields calculated from ERS-1 scatterometer wind observations, The Global Atmosphere and Ocean System, 6, 373–396, 1998.

Bentamy, A., Queffeulou, P., Quilfen, Y., and Katsaros, K.: Ocean surface wind fields estimated from satellite active and passive microwave instruments, IEEE Trans. Geosci. Remote Sens., 37, 2469–2486, 1999.

Bentamy A., Katsaros, K. B., Alberto, M., Drennan, W. M., and Forde, E. B.: Daily surface wind fields produced by merged satellite data, American Geophys. Union, 343–349, 2002.

Bentamy A., Ayina, H. L., and Queffeulou, P.: Investigation of the accuracy of the gridded satellite wind fields over the Mediterranean Sea: Comparisons with ECMWF wind estimates, MFSTEP report 3330, (http://www.bo.ingv.it/mfstep/WP3/), 2005.

Bourassa, M. A., Legler, D. M., O'Brien, J. J., and Smith, S. R.: SeaWinds validation with research vessels, J. Geophys Res., 108(C2), 3019, 2003.

Boutin, J., Etcheto, J., Rafizadeh, M., and Bakker, D. C. E.: Comparison of NSCAT, ERS 2 active microwave instrument, special sensor microwave imager, and Carbon Interface Ocean Atmosphere buoy wind speed: Consequences for the air-sea CO2 exchange coefficient, J. Geophys. Res., 104, 11 375–11 392, 1999.

Brody, L. R. and Nestor, M. J. R.: Regional Forecasting Aids for the Mediterranean Basin (Handbook for Forecasters in the Mediterranean, Part 2).Naval Research Laboratory, 7 Grace Hopper Avenue, Monterey, California, 93943-5502, 178 pp, 1980.

Chen, G.: An Intercomparison of TOPEX, NSCAT, and ECMWF Wind Speeds: Illustrating and understanding Systematic Discrepancies, Mon. Wea. Rev., 132(3), 780–792, 2003.
Crapolicchio, R., Lecomte, P., and Hersbach, H.: Assimilation of reprocessed ERS scatterometer data into ECMWF weather analysis on the Mediterranean Sea, Adv. Geosci., 2, 327–329, 2005.
Ebuchi, N., Graber, H. C., and Caruso, M. J.: Evaluation of wind vectors observed by QuikSCAT/SeaWinds using ocean buoy data, J. Atmos. Oceanic Tech., 19, 2049–2062, 2002.
Gaffard, C. and Roquet, H.: Impact of ERS-1 scatterometer wind data on the ECMWF 3D-Var assimilation system, Tech Memorandum no 217, ECMWF, 1995.
Goodberlet, M. A., Swift, C. T., and Wilkerson, J. C.: Remote sensing of ocean surface winds with the Special Sensor Microwave/Imager, J. Geophys. Res., 94, 14 547–14 555, 1989.
JPL: QuikScat science data product user's manual (version 2.0). Jet Propulsion Laboratory Publ. D-18053, Pasadena, CA, 84pp, (available online at http://podaac.jpl.nasa.gov/quikscat), 2001.
Komen, G. J., Cavaleri, L., Donelan, M., Hasselmann, K., Hasselmann, S., and Janssen, P. A. E. M.: Dynamics and Modelling of Ocean Waves, Cambridge University Press, 532p, 1994.
Long, D. E. and Mendel, J. M.: Identifiability in wind estimation from wind scatterometer measurements, IEEE Trans. Geosci. Remote Sens., GE-29, 268–276, 1991.
Meissner, T., Smith, D., and Wentz, F. J.: A 10-year intercomparison between collocated SSM/I oceanic surface wind speed retrievals and global analyses, J. Geophys. Res., 106(C6), 11 731–11 742, 2001.
Mestas-Nunez, A. M., Chelton, D. B., Freilich, M. H., and Richman, J. G.: An evaluation of ECMWF-based climatological wind stress fields, J. Phys. Oceanogr., 24, 1532–1549, 1994.
Monahan, A. H.: The Probability Distribution of Sea Surface Wind Speeds Part II: Data set Intercomparison and Seasonal Variability, J. Climate, 19(4), 521–534, 2006.
Picket, M. H., Tang, W., Rosenfeld, L. K., and Wash, C. H.: QuikSCAT satellite comparisons with nearshore buoy wind data off the U.S. west coast, J. Atmos. Oceanic Tech., 20, 1869–1979, 2003.
Portabella, M. and Stoffelen, A.: A comparison of KNMI quality control and JPL rain flag for SeaWinds, Can. Jour. of Rem. Sens., 28(3), 424–430, 2002.
Queffeulou, P.: Wave height variability over the Mediterranean Sea, using altimeter data, Proceedings of the Fifth International Symposium on Ocean Wave Measurements and Analysis,

Waves 2005, Madrid, 3–7 July, 2005.
Sobieski, P. W., Craeye, C., and Bliven, L. F.: Scatterometric signatures of multivariate drop impacts on fresh and salt water surfaces, Int, J. Remote Sens., 20, 2149–2166, 1999.

Table 1. Statistical parameters of Off-line and NRT wind speed and wind direction differences according to the use of three rain flags.

	Wind Speed			Wind Direction		
	Bias	Rms	Correlation	Bias	Std	Correlation
NRT flag	0.03	0.67	0.98	–2	22	1.78
NRT and off-line flag	0.00	0.51	0.99	–1	19	1.85
NRT and KNMI flag	0.02	0.51	0.99	–1	22	1.84

Table 2. Example of variogram parameters estimated for wind speed, zonal wind component, meridional component differences (Satellite – ECMWF) over three oceanic 5° box and during 2004 winter and summer seasons. The box is centered at 5° intervals of longitude and longitude 4° E–42° N. Numbers within brackets defined the 95% confidence interval.

		Wind Speed			Zonal Wind			Meridional Wind		
		a	*b*	*c*	*a*	*b*	*c*	*a*	*b*	*c*
Winter	Mediterranean sea	2.75 [2.54 2.97]	116 [66 166]	19 [11 28]	4.55 [3.92 5.17]	171 [72 271]	29 [12 45]	5.52 [5.07 5.98]	223 [157 288]	37 [26 48]
Summer	Mediterranean sea	2.26 [2.12 2.41]	163 [116 209]	27 [19 35]	4.17 [3.72 4.06]	270 [180 360]	45 [30 60]	3.89 [3.55 4.22]	244 [174 315]	41 [29 52]

Table 3. Mean and root mean square (Rms) difference values, and correlation values characterizing satellite and blended wind speed, zonal and meridional wind component comparisons. Same statistical parameters are provided for satellite and ECMWF comparisons.

		Bias (m/s)	Rms (m/s)	Cor
Wind Speed	Satellite/ Blended	0.00	0.25	0.99
	Satellite/ ECMWF	0.96	1.84	0.96
Zonal Component	Satellite/ Blended	0.00	0.24	0.99
	Satellite/ ECMWF	0.28	2.42	0.92
Meridional Component	Satellite/ Blended	0.00	0.25	0.99
	Satellite/ ECMWF	–0.30	2.26	0.96

Table 4. WMO ID and positions of moored buoy use to investigate the quality of Blended wind data.

Basin	Buoy	Position (latitude, longitude)
Mediterranean Sea	61001	43.40° N, 7.80° E
	61002	42.10° N, 4.70° E
	2008010	36.23° N, 5.03° W
	2029012	36.57° N, 2.34° W
	2077055	41.91° N, 3.65° E
	2083038	39.73° N, 4.42° E
	3155039	43.63° N, 3.05° W
Atlantic ocean	62001	45.20° N, 5.00° W
	1050076	44.06° N, 7.61° W
	1052046	44.06° N, 6.96° W
	3002002	42.12° N, 9.40° W
	3007036	43.49° N, 9.21° W
	3080042	43.73° N, 6.16° W

Table 5. Statistics between winds derived from buoy measurements, blended products, ECMWF analysis, QuikScat and SSM/I observations.

		Mediterranean				Atlantic			
		Bias	Std	Cor	N	Bias	Std	Cor	N
Wind Speed	Buoy/ Blended	–0.41	2.61	0.85	387	–0.34	1.92	0.86	790
	Buoy/ECMWF	1.59	1.96	0.82	387	0.30	1.56	0.92	790
	Buoy/QuikScat	–0.43	2.13	0.92	93	–0.21	1.62	0.91	189
	Buoy / SSMI	0.13	2.68	0.90	71	–0.18	2.26	0.76	150
Zonal Comp.	Buoy/ Blended	0.01	3.42	0.83	387	–0.57	2.18	0.92	790
	Buoy/ECMWF	–0.92	2.65	0.91	387	–0.37	1.90	0.94	790
	Buoy/QuikScat	–0.28	4.28	0.76	93	–0.14	2.57	0.90	189
Meridional Comp.	Buoy/ Blended	–0.81	2.86	0.88	387	–0.96	2.52	0.91	790
	Buoy/ECMWF	–0.06	1.94	0.93	387	–0.54	2.00	0.94	790
	Buoy/QuikScat	–0.91	4.01	0.84	93	–0.91	2.60	0.90	189

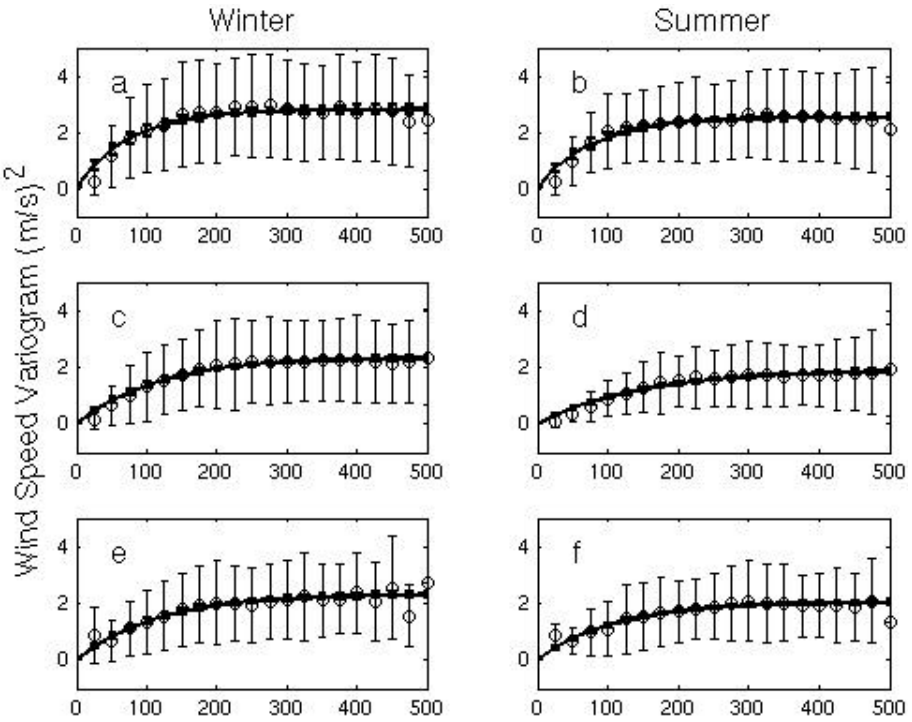

Fig. 1. Variogram function of $\tilde{\varepsilon}$ variable estimated over 5°×5° boxes in the Mediterranean sea for lag time less than 1 h. The box is centered at 5° intervals of longitude and longitude 4° E–42° N. The spatial structure is estimated for wind speed (**a** and **b**), zonal wind component (**c** and **d**), and for meridional component (**e** and **f**). The figures show the behavior of the variogram as a function of spatial separation (in km) estimated for winter and summer seasons.

OSD
3, 435–470, 2006

EGU

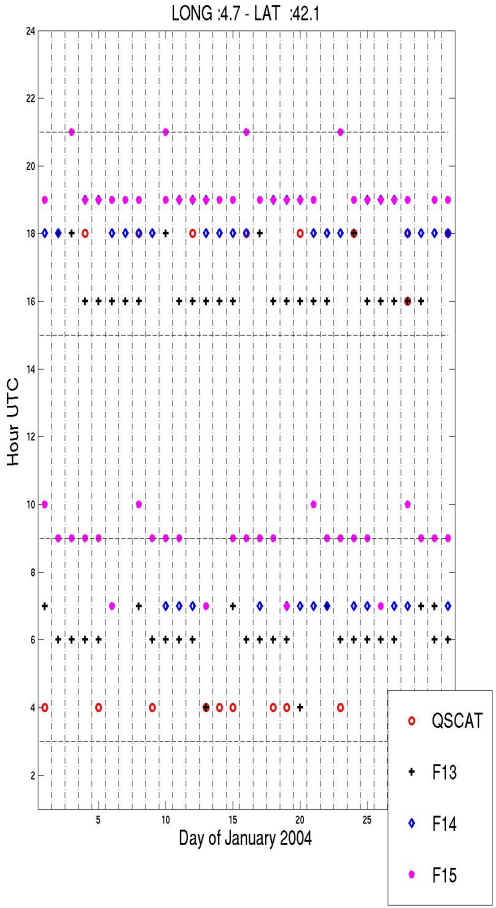

Fig. 2. Remotely sensed wind data availability during January 2004 and as function of UTC hour at the Mediterranean location 42.10° N–4.70° E.

OSD

3, 435–470, 2006

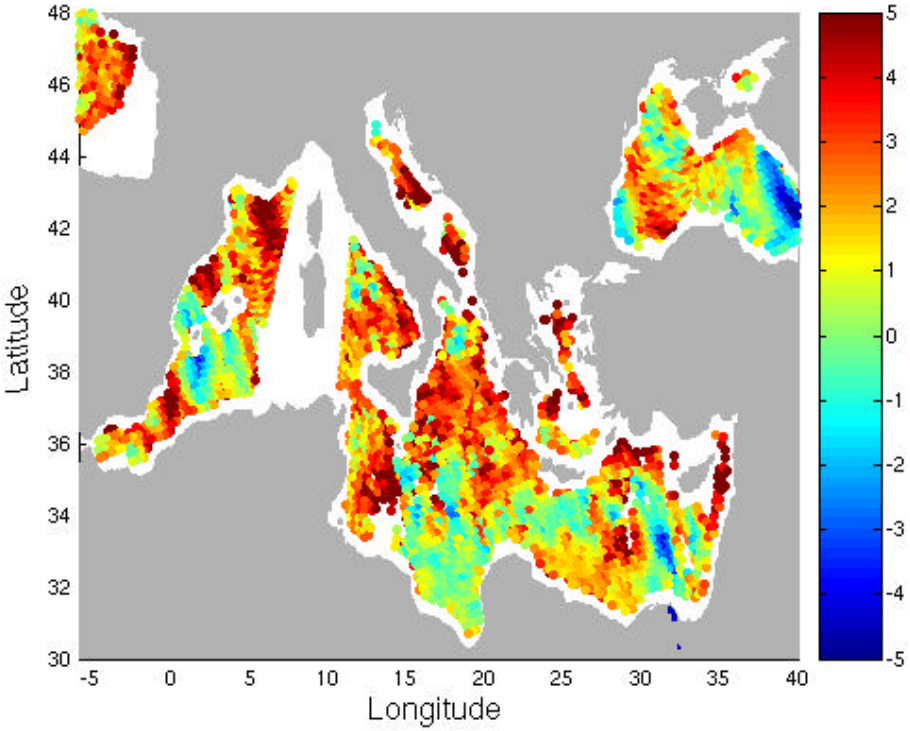

Fig. 3. Example of $\tilde{\varepsilon}_w$ observations (remotely sensed (QuikScat and SSM/I) – ECMWF wind speed in m/s) during the period 1 January 2004 03:00 a.m.–09:00 a.m.

OSD

3, 435–470, 2006

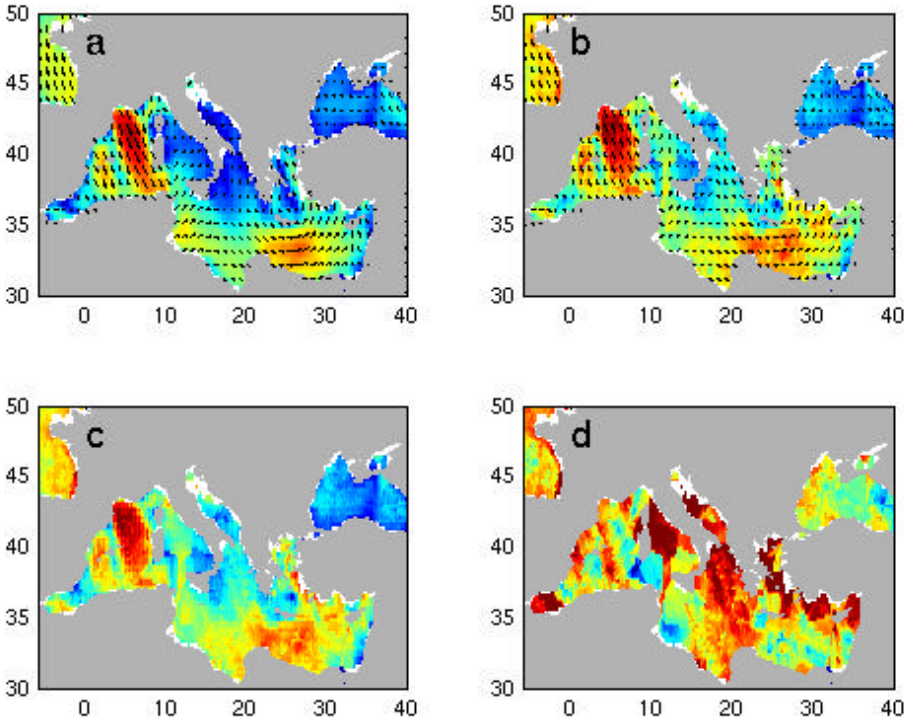

Fig. 4. Example of blended method result obtained for 2 January 2004 12:00 h: **(a)** ECMWF surface wind analysis; **(b)** blended wind product; **(c)** remotely sensed wind speed observations; **(d)** remotely sensed minus ECMWF wind speeds. Wind speed is ranged between 0 m/s (blue color) and 20 m/s (red color), while wind speed difference is ranged between –5 m/s and 5 m/s.

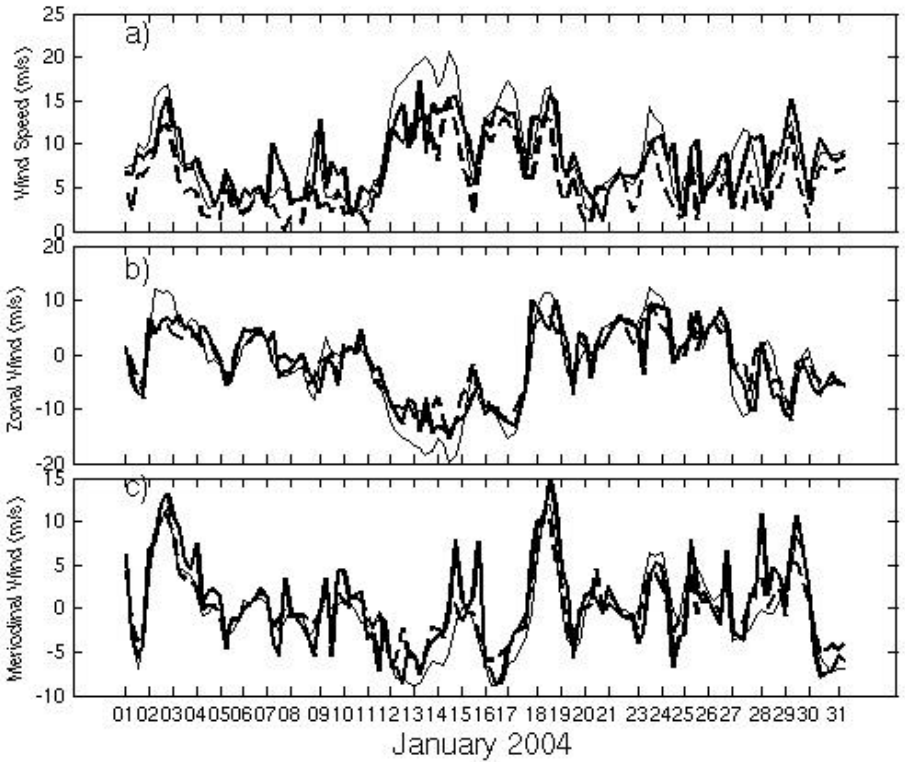

Fig. 5. Time series of wind speed **(a)**, zonal wind component **(b)**, and meridional wind component **(c)** derived from buoy (light line), blended product (heavy line), and from ECMWF analysis (dashed line) at buoy location 43.40° N–7.80° E (buoy 61001).

OSD
3, 435–470, 2006

EGU

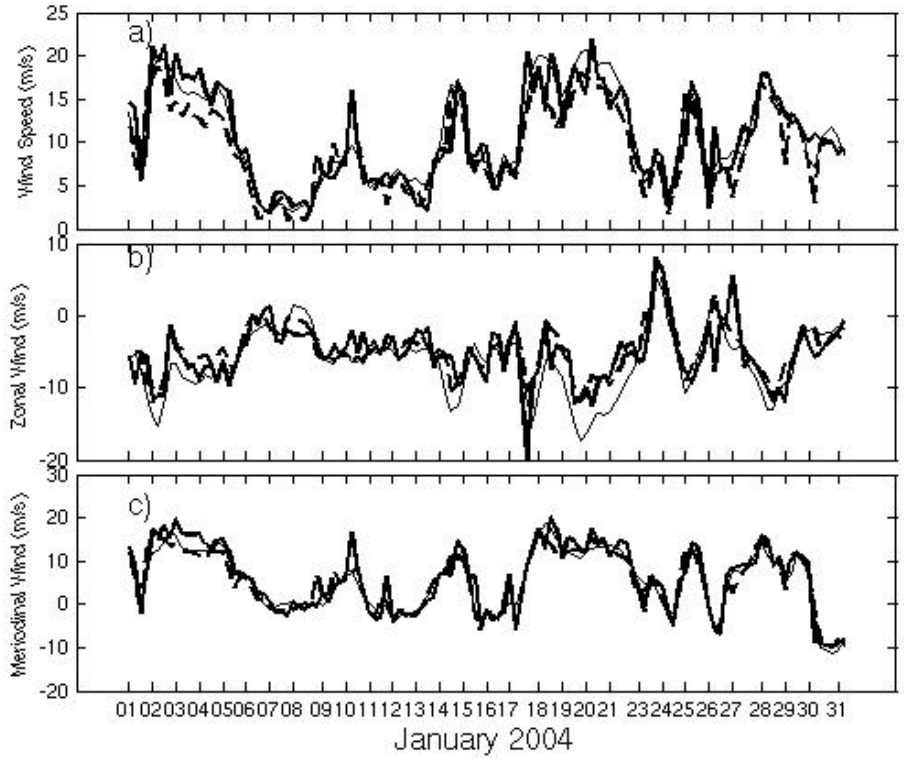

Fig. 6. As Fig. 5 at buoy location 42.10° N, 4.70° E (buoy 61002).

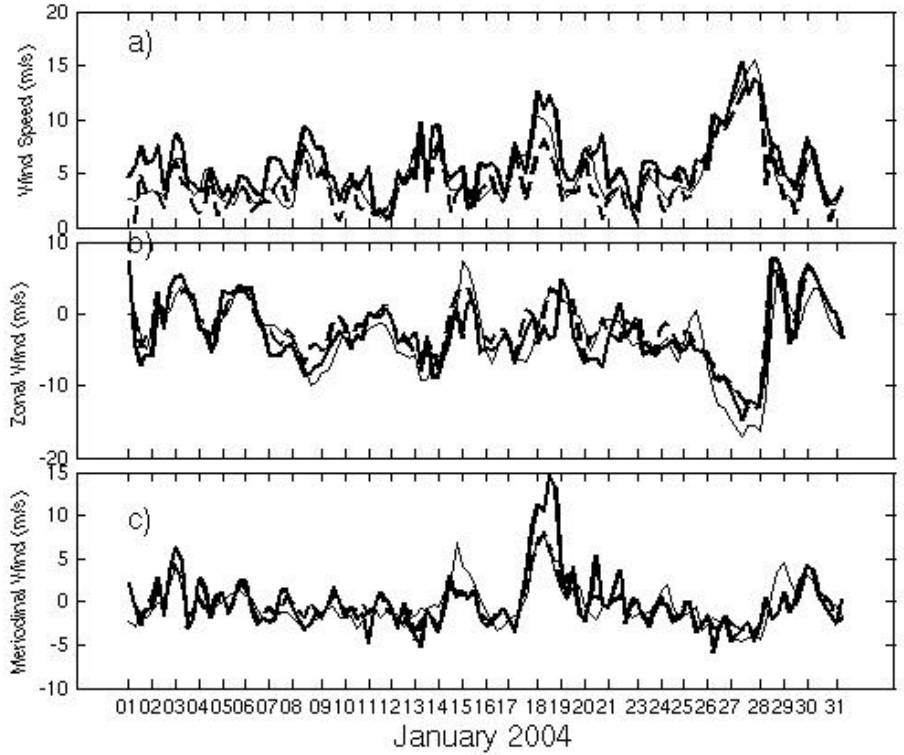

Fig. 7. As Fig. 5 at buoy location 36.57° N–2.34° W (buoy 2029012).